INT. J. REMOTE SENSING, 2002, VOL. 23, NO. 3, 461–475

Taylor & Francis
Taylor & Francis Group

Extraction of linear objects from interferometric SAR data

OLAF HELLWICH†*, IVAN LAPTEV‡ and HELMUT MAYER†

†Chair for Photogrammetry and Remote Sensing, ‡Forschungsgruppe Bildverstehen, Informatik IX, Technische Universität München, D-80290 Munich, Germany

(*Received 3 March 1999; in final form 11 September 2000*)

Abstract. A new method for the automated extraction of pipelines and other linear objects from Synthetic Aperture Radar (SAR) scenes is presented. It combines intensity data with coherence data from an interferometric evaluation of a SAR scene pair. The fusion is based on Bayesian statistics and is part of a Markov random field (MRF) model for line extraction. Both intensity and coherence data are evaluated using rotating templates. The different statistical properties of intensity and coherence are taken into account by a multiplicative noise model and an additive noise model respectively. The MRF model introduces prior knowledge about the continuity and the narrowness of lines. Posterior odds resulting from the MRF method are input to a method based on ziplock snakes for linear object extraction. This processing step is controlled interactively which is necessary as fully automatic processing of the given noisy data does not provide sufficiently predictable results. The method is applied to data of the ERS tandem mission.

1. Introduction

The extraction of linear objects such as roads, rivers and pipelines from SAR data is of great practical interest, because of the all-weather availability of SAR data. Its automation is not easy owing to the general speckle effect and 'no-show' effects for linear features (Leberl 1990). The newly developed method for linear object extraction tries to compensate for these defects as follows. SAR intensity and interferometric coherence data are combined in a Bayesian data fusion. An MRF model is used to bridge line gaps caused by speckle effects, thus considering the characteristics of SAR data. In the following processing, object extraction methods primarily developed for optical data are applied. In particular, interactively initialized ziplock snakes are used for linear object extraction.

In the following two sections the basics of MRF- and snake-based line extraction are explained. Then the method is applied to an ERS tandem data set from the Siberian lowlands for pipeline and railroad extraction.

2. MRF-based line extraction

Previous investigations have shown (Hendry *et al.* 1988, Hellwich and Streck 1996) that SAR intensity and coherence contain complementary information about

*Email: olaf@photo.verm.tu-muenchen.de

International Journal of Remote Sensing
ISSN 0143-1161 print/ISSN 1366-5901 online © 2002 Taylor & Francis Ltd
http://www.tandf.co.uk/journals
DOI: 10.1080/01431160110046750

linear objects. Over the whole scene both data sources are only weakly correlated. Visual inspections reveal that linear objects are often only visible in either intensity or coherence. To fuse the information contained in both data sources, an automatic method for data fusion was developed based on a Bayesian approach.

According to Bayes' theorem

$$p(\boldsymbol{\varepsilon}|\mathbf{y}) \propto p(\mathbf{y})\boldsymbol{\varepsilon})p(\boldsymbol{\varepsilon}) \tag{1}$$

the *a posteriori* probability density $p(\boldsymbol{\varepsilon}|\mathbf{y})$ of the object parameters $\boldsymbol{\varepsilon}$ given the observations $\mathbf{y}$ is proportional to the product of the probability density $p(\mathbf{y}|\boldsymbol{\varepsilon})$ of the observations given the object parameters and the *a priori* probability density $p(\boldsymbol{\varepsilon})$ of the object parameters. Considering that the observations are a constant in the estimation of object parameters, $p(\mathbf{y}|\boldsymbol{\varepsilon})$ is also called the likelihood function of the object parameters.

Bayes' theorem can also be applied recursively by using the *a posteriori* probability density $p(\boldsymbol{\varepsilon}|\mathbf{y}_1)$ belonging to the vector of observations $\mathbf{y}_1$ as *a priori* probability density for the evaluation of a second vector of observations $\mathbf{y}_2$ (Koch 1990, p. 8). If $\mathbf{y}_1$ and $\mathbf{y}_2$ are conditionally independent, the *a posteriori* probability is given by

$$\begin{aligned} p(\boldsymbol{\varepsilon}|\mathbf{y}_1, \mathbf{y}_2) &\propto p(\mathbf{y}_2\,\boldsymbol{\varepsilon})p(\boldsymbol{\varepsilon}|\mathbf{y}_1) \\ &\propto p(\mathbf{y}_2\,\boldsymbol{\varepsilon})p(\mathbf{y}_1|\boldsymbol{\varepsilon})p(\boldsymbol{\varepsilon}) \end{aligned} \tag{2}$$

In the newly developed method the observation vectors $\mathbf{y}_1$ and $\mathbf{y}_2$ contain values of the pixels of the SAR intensity and coherence images. The object parameters $\boldsymbol{\varepsilon}$ to be estimated for each pixel are the line or no-line state and—in case of the line state—the line direction. The *a priori* probability density $p(\boldsymbol{\varepsilon})$ of the object parameters is formulated as an MRF. In a MRF the probability of a state in a pixel s does not depend on the states of all other pixels of the image, but only on the states of pixels belonging to a neighbourhood ∂s of s.

The goal of processing is the computation of a vector of object parameters, i.e. line states and directions as well as no-line states for the pixels of the image, for which $p(\boldsymbol{\varepsilon}|\mathbf{y}_1, \mathbf{y}_2)$ is maximum or at least very high. In a MRF this can be achieved with the help of various methods manipulating local probability densities. In this work, the local highest confidence first (LHCF) algorithm (Chou *et al.* 1993) has shown the best performance with respect to detection quality and computational speed.

Using the equivalence of MRF and neighbour Gibbs fields (Geman and Geman 1984, Winkler 1995), Bayes' theorem (1) can be formulated for the local probability density in a single pixel s:

$$p(\varepsilon_s|\partial\varepsilon_s, y_s) \propto p(y_s|\varepsilon_s) \cdot p(\varepsilon_s|\partial\varepsilon_s) \tag{3}$$

In neighbour Gibbs fields, probabilities are expressed as a function of energies H:

$$p(x) = \frac{1}{Z}\exp\{-H(x)\} \tag{4}$$

where Z is a normalizing constant. With (4), energies can be used instead of probabilities:

$$H_s(\varepsilon_s|\partial\varepsilon_s, y_s) = H_s(y_s|\varepsilon_s) + H_s(\varepsilon_s|\partial\varepsilon_s) \tag{5}$$

In the following the computation of the different energy terms will be treated. A complete and in-depth description of the method is given by Hellwich (1997).

2.1. *Data evaluation*

Line extraction is conducted using a template which consists of a line zone and two neighbouring side zones (Lopes *et al.* 1993). This simple line model assumes that the backscatter properties are homogeneous in the line zone as well as in the side zones. To evaluate the image data, the template is centred at each pixel. The likelihood that the centre pixel of the template has the line state rises when the contrast between the line zone and both side zones increases. A contrast between the side zones is permitted. Different line directions are treated by rotating the line zone. The data evaluation for each pixel results in the energy term $H_s(y_s|\varepsilon_s)$ where y_s is a measure of the contrast between line and side zones, i.e. a derived observation. H_s is computed for both intensity and coherence.

2.1.1. *Intensity*

SAR intensity data follows a multiplicative noise model (Goodman 1975, Caves 1993). Therefore, the normalized intensity ratio r as a measure of contrast between two homogeneous regions has a constant false alarm rate. It is given by

$$r = \min\left(\frac{I_1}{I_2}, \frac{I_2}{I_1}\right) \tag{6}$$

where I_1 and I_2 are the mean intensities of both regions.

The result of the evaluation of a template for a specific line direction is the maximum of the two normalized intensity ratios between the line zone and the side zones. This is the derived observation r_s in pixel s. Hence, the energy is given by

$$H_s(r_s|\varepsilon_s) = \begin{cases} r_s^2/2\sigma_r^2 \text{ if } \varepsilon_s \in L \\ t_r^2/2\sigma_r^2 \text{ if } \varepsilon_s = N \end{cases} \tag{7}$$

where σ_r is a constant and t_r is a threshold balancing the no-line state versus the line states. L comprises the set of line states with different line directions and N corresponds to the no-line state. Equation (7) was inspired by normally distributed observations. Empirical investigations (Hellwich 1997) have shown that it agrees sufficiently with the theoretically derived probability density of the normalized intensity ratio between homogeneous regions with a known contrast (Caves 1993, Lopes *et al.* 1993).

2.1.2. *Coherence*

The coherence γ does not follow a multiplicative noise model (Tough *et al.* 1995, Equation (87)). Figure 1 shows the probability density function of sample coherence for several coherence values. It can be seen that for low coherence values ($\gamma < 0.6$) the noise model is approximately additive, whereas for high coherence values ($\gamma > 0.6$) the noise model is rather multiplicative with respect to the decorrelation $1-\gamma$. In this work an additive noise model of coherence was assumed. This means that the difference d of the mean coherence values of the template zones has a constant false alarm rate and can be used as a measure of contrast between the regions. The derived observation d_s for a pixel s is the minimum of the coherence differences between the line zone and both side zones. Corresponding to (7), the energy for differences d_s is computed from

$$H_s(d_s|\varepsilon_s) = \begin{cases} (d_s - \mu_d)^2/2\sigma_d^2 \text{ if } \varepsilon_s \in L \\ (t_d - \mu_d)^2/2\sigma_d^2 \text{ if } \varepsilon_s = N \end{cases} \tag{8}$$

where μ_d is a very large coherence difference occurring in the evaluated data. It can be set relatively arbitrarily. t_d is a threshold balancing the no-line state versus the line states. σ_d is used for weighting the coherence data with respect to the intensity data.

2.2. *Markov random field model*

As the MRF model is not essential for the fusion of the two data sources, it is described very briefly only. The purpose of the model is the detection of continuous, thin lines. It is designed to bridge speckle-related, i.e. short, gaps interrupting the lines.

According to the model, each pixel with line state influences pixels in its neighbourhood. In a line pixel's direction it supports the presence of line pixels with a

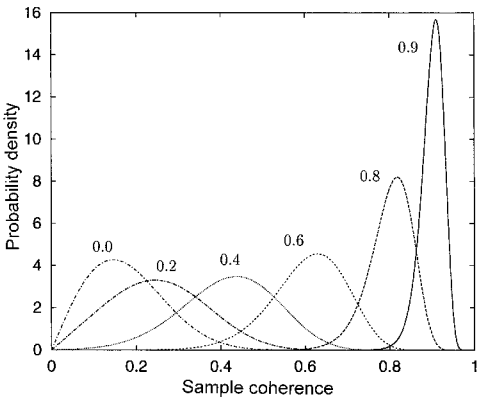

Figure 1. Probability density function of sample coherence for coherence values 0.0, 0.2, 0.4, 0.6, 0.8 and 0.9.

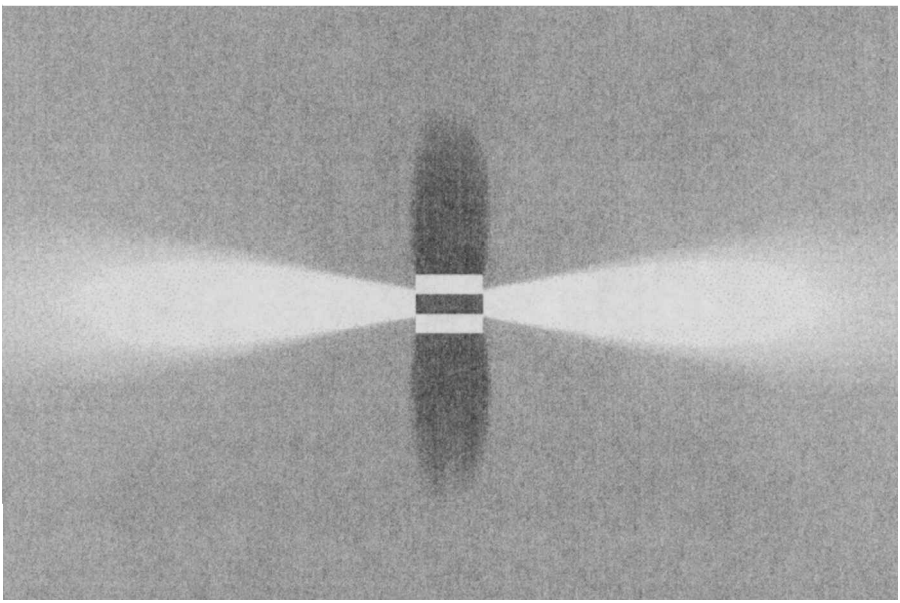

Figure 2. Model for the influence of a line pixel with horizontal direction (light, line-supporting field; dark, line-inhibiting field).

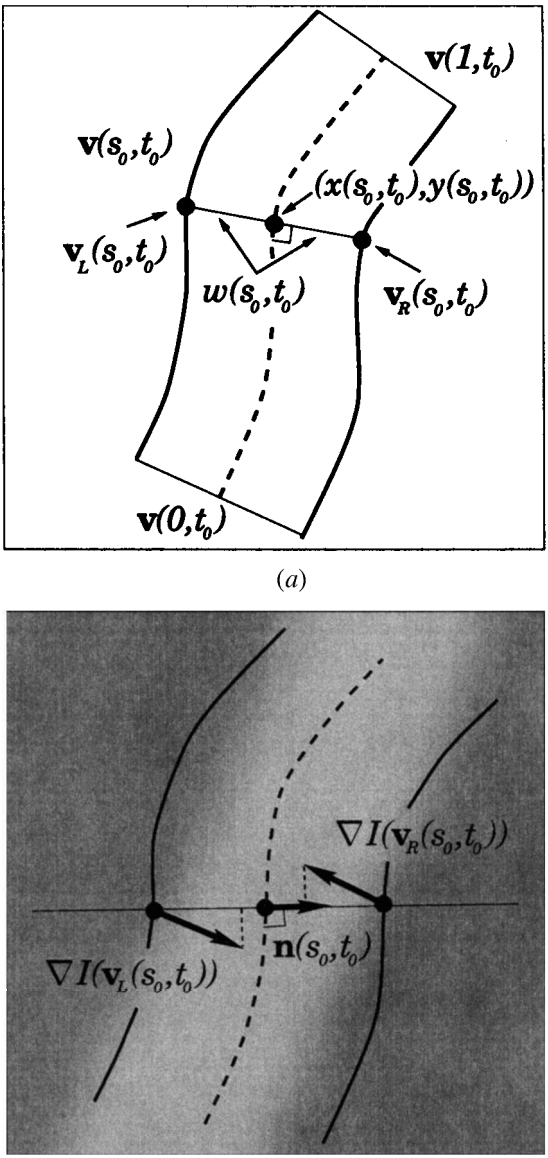

Figure 3. (*a*) Parametric representation of the ribbon snake. Each slice $\mathbf{v}(s_0, t_0)$ is identified by its centre $(x(s_0, t_0), y(s_0, t_0))$ and width $2w(s_0, t_0)$. (*b*) Image gradients for the two sides of the ribbon and their projection onto the ribbon's unit normal vector $\mathbf{n}(s_0, t_0)$.

corresponding line direction. The effect of this influence is a stronger line continuity, i.e. a closing of gaps. Perpendicularly to its direction a line pixel inhibits the presence of line pixels with the same direction, thus preventing the occurrence of thick lines. These two ways in which a line pixel influences its neighbourhood are modelled with the help of completion fields (Williams and Jacobs 1995) which the pixel 'radiates' (see figure 2). The two parameters of the model control the strengths of the field's

Figure 4. Multitemporal histogram-equalized magnitude (square root of intensity) of an ERS-SAR scene. Approximate scale of the figure is 1:130 000, the size of the area is $17 \times 17\,\mathrm{km}^2$. The geographic location of the site can be taken from figure 11.

supporting and inhibiting lines. They are also used to weigh the influence of the MRF prior to the data.

In summary, line extraction is controlled by the parameters t_r, t_d, and σ_d for data evaluation, and the line-supporting and the line-inhibiting parameter of the MRF model. By means of a training data set optimal parameters can be determined using simulated annealing (Hellwich 1998).

The results are line pixels with line directions and no-line pixels, as well as posterior odds of the most probable line state versus the no-line state for each pixel. The latter are used for the snake-based linear feature extraction explained in the next section.

3. Snakes

This section is based on the work of Laptev (1997) and Mayer *et al.* (1998), where details of the approach can be found.

Figure 5. Multitemporal histogram equalized coherence of the ERS-SAR tandem interferogram corresponding to figure 4. The geographic location of the site can be taken from figure 11.

3.1. *Basics of snakes*

The concept 'snake', also called 'active contour model', was originally introduced by Kass *et al.* (1987). It combines internal smoothness constraints like the bending of a curve with image forces like the gradient. This idea can be represented as a sum of its energies.

$$E(\mathbf{v}) = E_{\text{img}}(\mathbf{v}) + E_{\text{int}}(\mathbf{v}) \tag{9}$$

where E_{int} represents the *internal energy* and E_{img} the *image energy*. The position of the snake where all these forces compensate each other corresponds to the local minimum of the snake's total energy E. Thus, the problem of the optimization of the snake's position is equivalent to the minimization of its energy.

The image energy of the snake can be defined as:

$$E_{\text{img}}(\mathbf{v}) = -\int_0^1 P(\mathbf{v}(s, t))\mathrm{d}s \tag{10}$$

Figure 6. Line pixels (black) and no-line pixels (white) extracted from intensity data.

where $P(\mathbf{v}(s, t))$ is a function with high values corresponding to the features of interest. When attracting the snake to edges in images, $P(\mathbf{v}(s, t))$ is usually taken equal to the magnitude of the image gradient, i.e.

$$P(\mathbf{v}(s, t)) = |\nabla I(\mathbf{v}(s, t))| \tag{11}$$

where $I(\mathbf{v}(s, t))$ is the raw image or, more often, the image convolved with the Gaussian kernel. The convolution with a Gaussian kernel smoothes the image and removes disturbances which prevent the snake from moving toward the positions with lower image energy corresponding to more salient image features.

The internal energy makes it possible to introduce geometric constraints on the shape of the snake. It can be defined as

$$E_{\text{int}}(\mathbf{v}) = \frac{1}{2}\int_0^1 \alpha(s)\left|\frac{\partial \mathbf{v}(s, t)}{\partial s}\right|^2 + \beta(s)\left|\frac{\partial^2 \mathbf{v}(s, t)}{\partial s^2}\right|^2 \mathrm{d}s \tag{12}$$

where $\alpha(s)$ and $\beta(s)$ are arbitrary functions that control the snake's tension and rigidity respectively. The constraint on tension is introduced by the first-order term

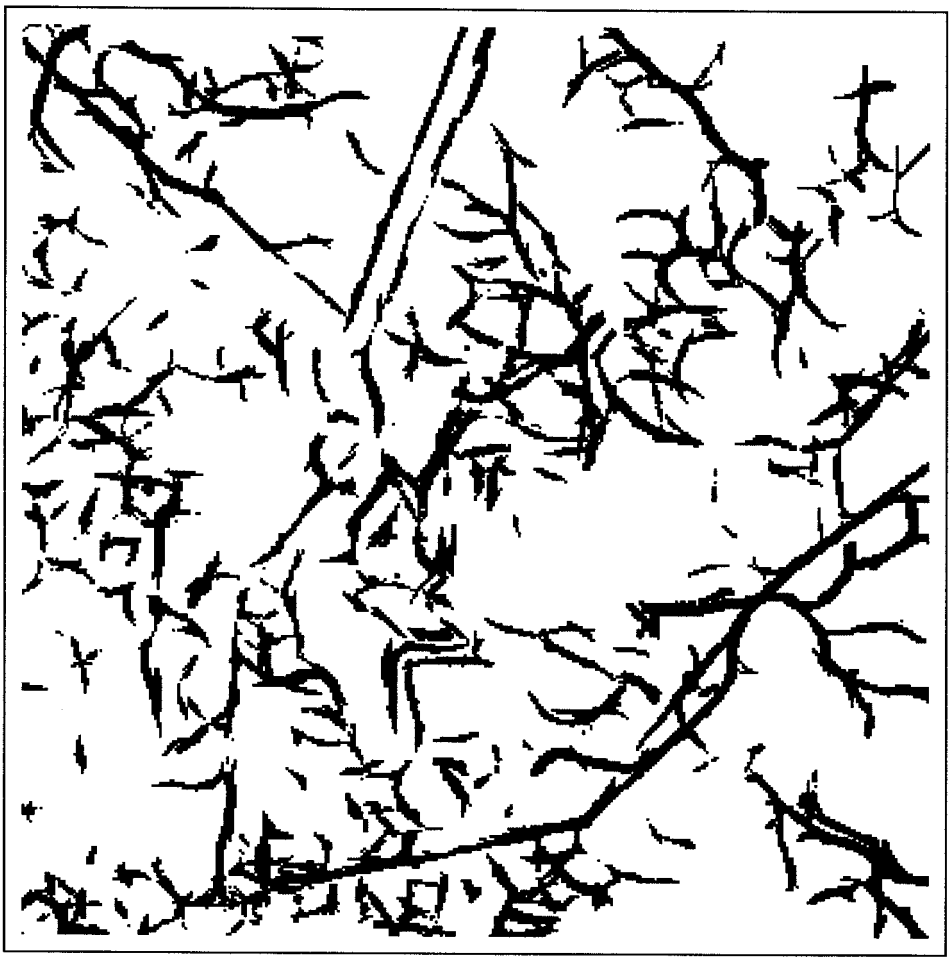

Figure 7. Line pixels (black) and no-line pixels (white) extracted from both intensity and coherence data.

and makes the snake act like a membrane. The rigidity is constrained by the second-order term and makes the snake act like a thin plate.

In order to find the optimal position for the snake, its energy has to be minimized. According to variational calculus this must be a solution to the Euler–Lagrange differential equation of motion. When choosing a particular deformation energy the differential equation controlling the motion of the snake becomes linear and can be separated. This has the advantage of solving one optimization step in linear time. For the actual implementation the equations have to be discretized.

3.2. *Ribbon snakes*

The goal of this work is to extract linear features with a small but significant width. They can be modelled by ribbons whose sides correspond to the features' boundaries. Using ribbon snakes, linear features can be extracted by optimizing the position and the width of the ribbon. In order to represent ribbon snakes, the

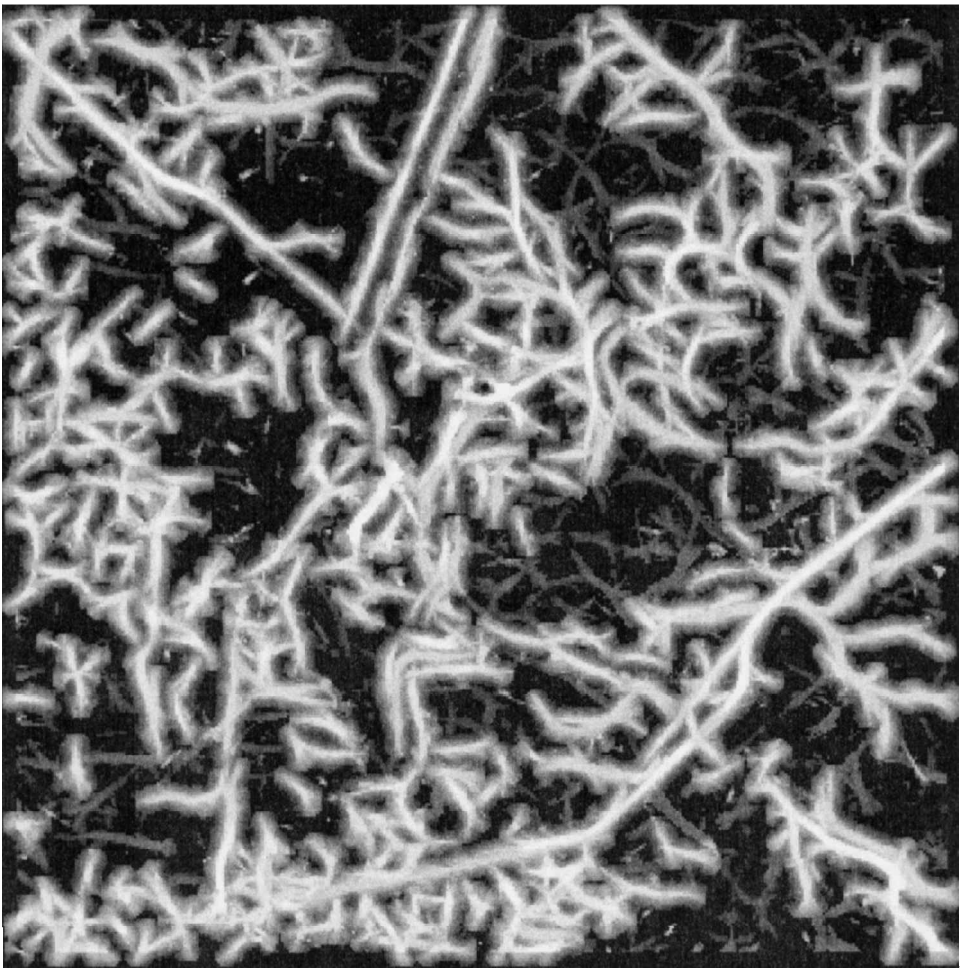

Figure 8. Posterior odds.

parametric curve $\mathbf{v}(s, t)$ is augmented by a third component $w(s, t)$ (Fua and Leclerc 1990):

$$\mathbf{v}(s, t) = (x(s, t), y(s, t), w(s, t)) \qquad (0 \leqslant s \leqslant 1) \tag{13}$$

This representation implies that each slice of the ribbon snake $\mathbf{v}(s_0, t_0)$ is characterized by its width $2w(s_0, t_0)$ and the location of its centre $(x(s_0, t_0), y(s_0, t_0))$. All centre points compose the centreline of the ribbon (see figure 3(*a*)).

In order to perform optimization of the ribbon snake, the forces which act on it have to be defined. The advantage of the ribbon's representation in equation (13) is that the expression for the snake's internal energy E_{int} can be directly used for ribbon snakes. Doing so, the width of ribbons will be constrained by tension and rigidity in the same way as the two coordinate components. The internal forces that act on the ribbon snake will on the one hand constrain the ribbon's centreline to be a smooth curve. On the other hand, they will control the distance between the ribbon's sides, forcing them to be parallel.

In contrast to the original snakes, the image information for ribbon snakes has

Figure 9. Pipelines and railroads extracted with ziplock snakes from posterior odds superimposed on the SAR magnitude image. The geographic location of the site can be taken from figure 11.

to be taken into account not at the centre of the curve $(x(s, t), y(s, t))$, but at the ribbon's left and right sides. As shown in figure 3(*a*), for each slice of the ribbon $\mathbf{v}(s_0, t_0)$ there exist two points $\mathbf{v}_L(s_0, t_0)$ and $\mathbf{v}_R(s_0, t_0)$ corresponding to the ribbon's left and right sides. Adapting the expression for image energy E_{img} in equation (10) to ribbon snakes, the function $P(\mathbf{v}(s, t))$ in equation (11) has to be redefined. Requiring the image contrast to be large along the left and the right side of the ribbon, P can be defined as the sum of the image gradient magnitudes on the left and right ribbon sides:

$$P(\mathbf{v}(s, t)) = |\nabla I(\mathbf{v}_R(s, t))| + |\nabla I(\mathbf{v}_L(s, t))| \tag{14}$$

However, when searching for linear features which are known to be brighter or darker than their surroundings, the result of the extraction can be improved if the direction of image gradients at the left and right side of the ribbon is also taken into consideration. For example, the extraction of bright linear features implies that the

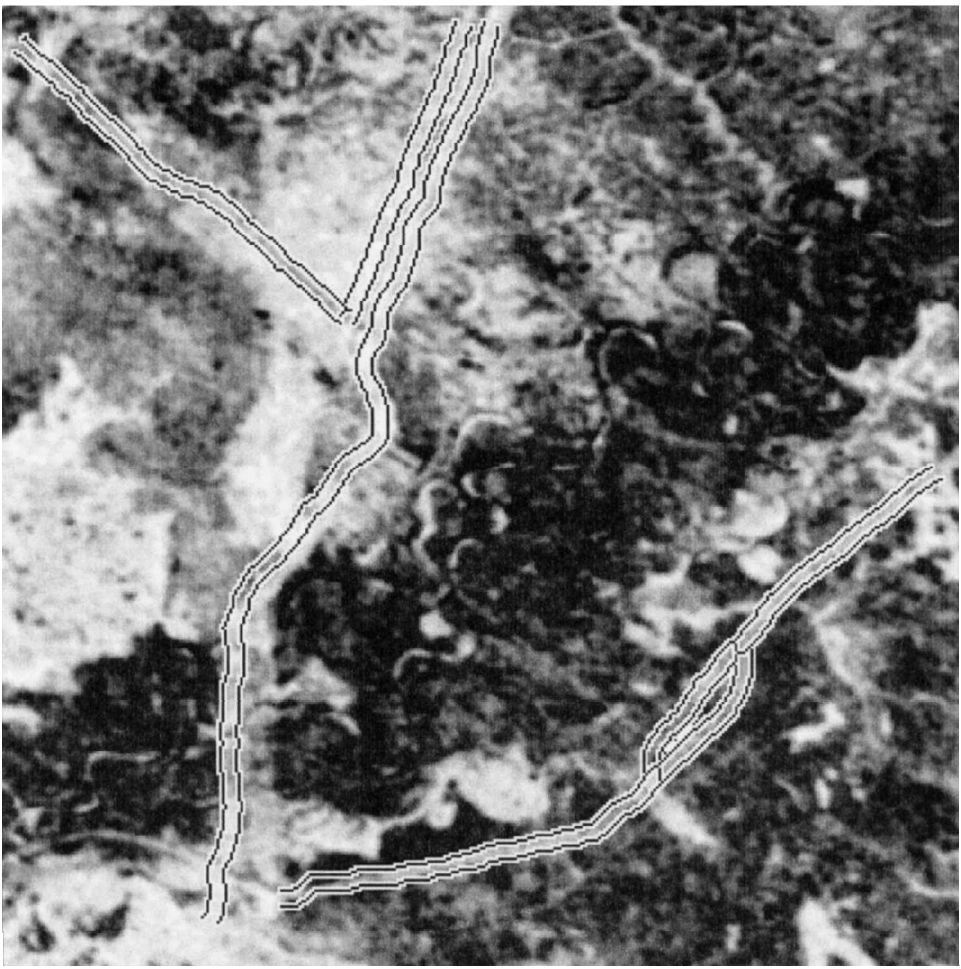

Figure 10. Pipelines and railroads extracted with ziplock snakes from posterior odds superimposed on the interferometric SAR coherence image. The geographic location of the site can be taken from figure 11.

image intensity at the ribbon sides has to change from dark to bright at the left ribbon side and from bright to dark at its right side (see figure 3(*b*)). This is equivalent to demanding the projection of image gradient on the vector $\mathbf{n}(s, t)$ to be negative along the ribbon's left side $\mathbf{v}_L(s, t)$ and positive along its right side $\mathbf{v}_R(s, t)$. Taking this into account, the function $P(\mathbf{v}(s, t))$ can be redefined as

$$P(\mathbf{v}(s, t)) = (\nabla I(\mathbf{v}_L(s, t)) - \nabla I(\mathbf{v}_R(s, t))) \cdot \mathbf{n}(s, t) \tag{15}$$

3.3. *Ziplock principle*

A problem often encountered is the following: to make human interaction as efficient as possible only the end points of the snake are given manually. Especially close to the centre, the direct straight connection of these end points can be far off from the, e.g. largely curved, linear object. This does not only make optimizing the whole snake at a time inefficient, but lets the snake get stuck in local minima. To overcome these problems, the 'ziplock' method was introduced by Neuenschwander *et al.* (1995). There,

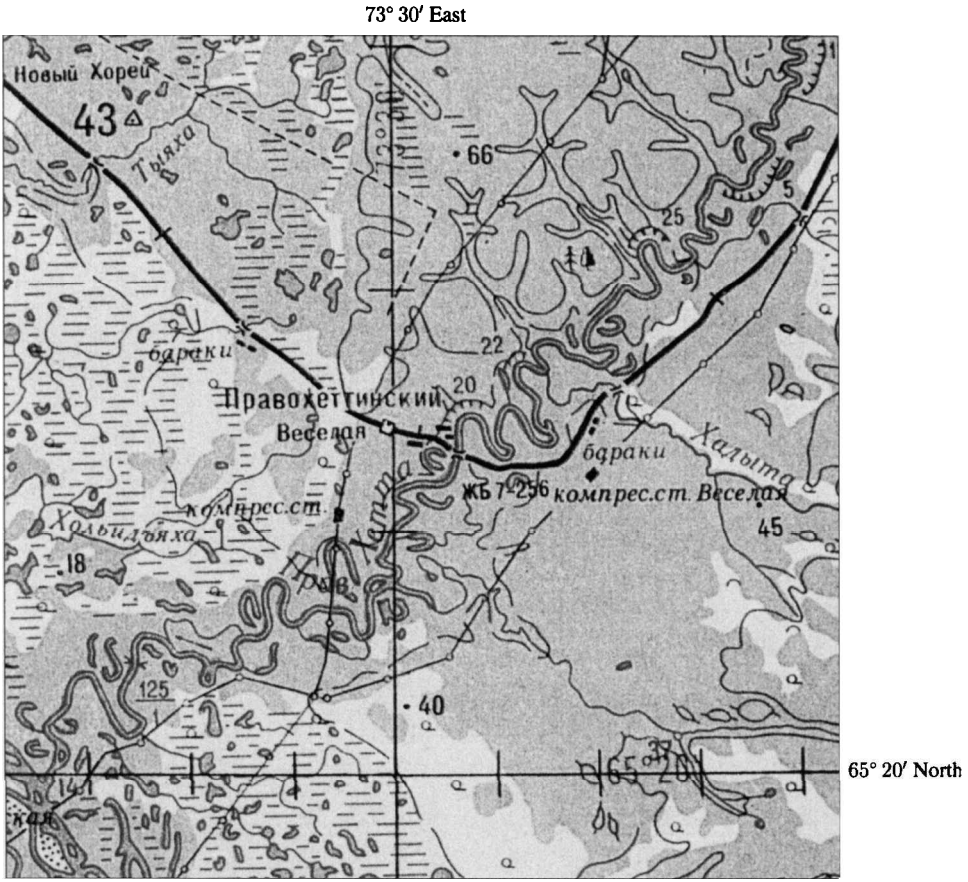

Figure 11. Section of the Russian topographic map 1:500 000. Approximate scale of the figure is 1:290 000, the size of the area $32 \times 32\,km^2$. The main town in the map section is Pravokhettinskiy near Veselaya railway station. ©Government of Russia.

information is gradually propagated from the ribbon's ends towards its centre by optimizing only parts of the snake at a time while approaching the centre. The curvature of the snake is constrained to be low. In this way the 'active' parts of the snake remain close to the linear feature during the whole optimization. The whole snake and the linear feature behave like a ziplock closed from both ends.

4. Results

As part of an ERS tandem data set from the Siberian lowlands at approximately 65° 20′ North and 73° 30′ East is used to demonstrate the feasibility of the new method. It contains straight oil pipelines and railroads. The pipelines were extracted as part of a project to investigate leaks in oil pipelines using ERS interferometric SAR data, i.e. they had to be treated separately from other anthropogeneous objects. Figure 4 shows the magnitude, i.e. square root of intensity which is visually easier to interpret than intensity itself, and figure 5 the coherence. In this case, both images are multitemporal data sets, i.e. they contain averages of several data takes. Though the developed method is not limited to this type of image, it was used as it provides an improved visibility of the relevant features.

Figures 6 and 7 display the line pixels extracted with the MRF method. The result presented in figure 6 is based on intensity data only. It can be seen that it does not contain the pipelines in the lower half of the image where they cross a river. This is different when the extraction is based on a combination of intensity and coherence data as displayed in figure 7.

The posterior odds of the most probable line states versus the no-line states are shown in figure 8. They combine the basic line information of intensity and coherence data, and are therefore input of the interactive ziplock snake-based pipeline extraction. Figures 9 and 10 present five extracted pipelines and railroads superimposed onto the magnitude and the coherence image respectively. Careful visual inspection reveals that a correct extraction of the pipelines would not have been possible with one of the data sources alone. The intensity does not contain any line information in the fluvial plain of the river, and the coherence does not show sufficient line information in the upper part of the image.

The ziplock method was of major importance for the success of the extraction based on ribbon snakes: only by optimizing from the given ends inwards was it possible to track the pipeline and avoid catching other lines with high posterior odds.

Figure 11 shows a section of a Russian topographic map (scale 1:500 000) containing the test area. The extraction results agree with the map contents. Minor differences could either be extraction errors or changes of the location asking for map updates. Inspection of the map reveals that it is extremely difficult to identify the railroad in the fluvial plain of the river.

5. Conclusions

The fusion of SAR intensity and interferometric SAR coherence data for line extraction using a Bayesian approach has been introduced. The new method applies the MRF model to suppress speckle-related line gaps. The results yield line pixels with line directions and posterior odds showing the strength of the line state in comparison with the no-line state.

The posterior odds contain line information from both data sources. They can be used for further object examination. Here, they have been input to an extraction of pipelines based on ziplock snakes. Though it would be desirable to conduct the extraction automatically, interactive processing was chosen to achieve reliable results. The reasons for difficulties of automatic processing are twofold. (1) Depsite the speckle suppressing effect of the MRF model, the posterior odds have a high noise level. They contain many features that are caused by objects other than pipelines, e.g. by terrain features such as valleys or river banks, which confuse automatic extraction. (2) The object model of the ziplock snake method has been developed for road extraction from optical imagery. It would possibly be more successful for automatic extraction if it had been better adjusted to the appearance of objects in SAR data.

So summarizing, it is advisable to use SAR data with a higher spatial resolution for the extraction of linear anthropogeneous objects rather than ERS imagery. Furthermore, it appears appropriate to supplement SAR intensity with interferometric coherence data wherever possible.

Acknowledgments

The authors thank Kayser-Threde GmbH, München, for providing the SAR data. This research was partially funded by Deutsches Zentrum für Luft- und

Raumfahrt DLR e.V. under grant 50EE9423 and by Deutsche Forschungsgemeinschaft DFG under grant Eb74/8-2.

References

CAVES, R., 1993, Automatic Matching of Features in Synthetic Aperture Radar Data to Digital Map Data. Dissertation, Dept. of Applied and Computational Mathematics, University of Sheffield.

CHOU, P. B., COOPER, P. R., SWAIN, M. J., BROWN, C. M., and WIXSON, L. E., 1993, Probabilistic Network inference for cooperative high and low level vision. In *Markov Random Fields. Theory and Applications*, edited by R. Chellappa and A. Jain (Boston: Academic Press), pp. 211–243.

FUA, P., and LECLERC, Y., 1990, Model driven edge detection. *Machine Vision and Applications*, **3**, 45–56.

GEMAN, D., and GEMAN, S., 1984, Stochastic relaxation, Gibbs distribution, and the Bayesian restoration of images. *IEEE Transactions on Pattern Analysis and Machine Intelligence*, **6**, 721–741.

GOODMAN, J. W., 1975, Statistical properties of laser speckle patterns. In *Laser Speckle and Related Phenomena, Vol. 9 of Topics in Applied Physics*, edited by J. C. Dainty (Berlin: Springer-Verlag), 9–74.

HELLWICH, O., 1997, Linienextraktion aus SAR-Daten mit einem Markoff-Zufallsfeld-Modell, Vol. 487 of *Reihe C* (München: Deutsche Geodätische Kommission).

HELLWICH, O., 1998, Model parameter estimation using simulated annealing. *International Archives of Photogrammetry and Remote Sensing*, **33**, pp. 233–238.

HELLWICH, O., and STRECK, C., 1996, Linear structures in SAR coherence data. *Proceedings of International Geoscience and Remote Sensing Symposium '96, Lincoln, 27–31 May 1996*, Vol. I (Piscataway, NJ: IEEE), pp. 330–332.

HENDRY, A., QUEGAN, S., and WOOD, J., 1988, The visibility of linear features in SAR images. *International Geoscience and Remote Sensing Symposium 88, Edinburgh, 13–16 September 1988* (Piscataway, NJ: IEEE), pp. 1517–1520.

KASS, M., WITKIN, A., and TERZOPOULOS, D., 1987, Snakes: active contour models. *International Journal of Computer Vision*, **1**, 321–331.

KOCH, K.-R., 1990, *Bayesian Inference with Geodetic Applications*, *Lecture Notes in Earth Sciences, No. 31* (Berlin: Springer-Verlag).

LAPTEV, I., 1997, Road Extraction Based on Snakes and Sophisticated Line Extraction. Master's Thesis, Computational Vision and Active Perception Lab (CVAP), Royal Institute of Technology, Stockholm, Sweden.

LEBERL, F. W., 1990, *Radargrammetric Image Processing* (Norwood, MA: Artech House).

LOPES, A., NEZRY, E., TOUZI, R., and LAUR, H., 1993, Structure detection and statistical adaptive speckle filtering in SAR images. *International Journal of Remote Sensing*, **14**, 1735–1758.

MAYER, H., LAPTEV, I., and BAUMGARTNER, A., 1998, Multi-scale and snakes for automatic road extraction. In *Computer Vision – ECCV'98*, edited by H. Burkhardt and B. Neumann (Berlin: Springer-Verlag), pp. 720–733.

NEUENSCHWANDER, W., FUA, P., SZÉKELY, G., and KÜBLER, O., 1995, From Ziplock snakes to Velcro™ surfaces. *Automatic Extraction of Man-Made Objects From Aerial and Space Images* (Basel: Birkhäuser Verlag), pp. 105–114.

TOUGH, R. J. A., BLACKNELL, D., and QUEGAN, S., 1995, A statistical description of polarimetric and interferometric synthetic aperture radar data. *Proceedings of the Royal Society of London* A, **449**, 567–589.

WILLIAMS, L., and JACOBS, D., 1995, Stochastic completion fields: a neural model of illusory contour shape and saliency. *Fifth International Conference on Computer Vision, Cambridge, MA, USA, 20–22 June 1995* (Piscataway, NJ: IEEE), pp. 408–415.

WINKLER, G., 1995, *Image Analysis, Random Fields and Dynamic Monte Carlo Methods*, Vol. 27 of *Applications of Mathematics* (Berlin: Springer-Verlag).